Catalysis Letters Vol. 108, Nos. 3–4, May 2006 (© 2006)
DOI: 10.1007/s10562-006-0047-5

Improved performance of Au/Fe_2O_3 catalysts promoted with ZrO_2 and Nb_2O_5 in the WGS reaction under hydrogen-rich conditions

Fengli Zhang,[a] Qi Zheng,[a,*] Kemei Wei,[a] Xingyi Lin,[a] Hanhui Zhang,[b] Jinwei Li,[a] and Yanning Cao[b]

[a]*National Engineering Research Center of Chemical Fertilizer Catalysts, Fuzhou University, Gongye Road 523, Fuzhou 350002, China*
[b]*Department of Chemistry, Fuzhou University, Fuzhou, Fujian 350002, China*

Received 10 January 2006; accepted 21 February 2006

Effect of addition of the ZrO_2 and Nb_2O_5 promoters on the activity and stability of the Au/Fe_2O_3 catalysts in the WGS reaction under hydrogen-rich conditions was studied. Results showed that this new catalyst possesses enhanced activity and stability under conditions common in fuel processors. Its CO conversion almost reached the maximum value 99% at 200 °C and maintained better stability compared with unmodified samples within 50 h on-stream. Detailed characterization including BET, XRD, HRTEM, XPS, XRF and H_2-TPR revealed that ZrO_2 and Nb_2O_5 acted as structural promoters and a strong interaction between ZrO_2 and Nb_2O_5 existed. The enrichment of Zr and Nb on the surface kept the gold and magnetite particles apart delaying sintering. More active gold sites, larger surface area and smaller magnetite particles were the main reasons for the enhanced performance.

KEY WORDS: gold; iron oxide; zirconium oxide; niobium oxide; water–gas shift; promoters.

1. Introduction

The water gas shift (WGS) reaction, $CO + H_2O \leftrightarrow CO_2 + H_2$ is an industrially important route to H_2 production and plays an essential role in many current technologies such as the rapidly developing fuel cell technology, an efficient and clean alternative to fuel combustion for primary power generation [1]. Although platinum group metals (PGM) have been employed as the most effective and durable catalysts within most types of low temperature fuel cells [2–4], the high price and limited availability of platinum becomes one of the major barriers to commercialization of fuel cells. Research has also shown that supported gold catalysts are very active in the WGS reaction at low temperatures [5, 6], thus potential candidates for use in fuel processors. However, most of previous studies on gold-based catalysts used a mixture of carbon monoxide and inert gases as feed [7–11], and therefore are not applicable to the hydrogen-rich conditions prevailing in the fuel cell systems. In fact, the fast deactivation of gold catalysts under synthetic and real reformate tests has been reported. The studies by Kim and Thompson showed that despite the high initial activity, Au/CeO_2 catalysts lost activity by more than 50% during the first 12 h in a simulated reformate mixture (10% CO, 22% H_2O, 6% CO_2, 43% H_2 and 19% N_2) [12]. The deactivation maybe caused by the presence of large amount of H_2 [13].

Therefore, the development of gold catalysts which are able to maintain high activity and stability under hydrogen-rich conditions has become one of the current technical challenges for fuel cell catalyst industry. Considerable efforts including the selection of the appropriate supports and the choice of the preparation method have been made to design the highly efficient catalysts. Until today, less effort, however, was made to investigate the suitable promoters used Au/Fe_2O_3 catalyst. In this study, we developed an improved formulation of Au/Fe_2O_3 catalysts by simultaneously adding the promoters ZrO_2 and Nb_2O_5. Performance tests carried out in the reformed methane steam showed that this new catalyst possesses enhanced activity and stability under conditions common in fuel processors.

*To whom correspondence should be addressed.
E-mail: qizheng2005@gmail.com

2. Experimental

2.1. Catalyst preparation

A series of samples with varied Nb_2O_5 contents (1, 3, 5, 8, 10 wt%) and fixed Au (8 wt%) and ZrO_2 (10 wt%) loadings were prepared by parallel co-precipitation method and labeled as AuFZN1, AuFZN3, AuFZN5, AuFZN8 and AuFZN10, respectively. As controls, we also made Au/Fe_2O_3 samples without any promoters, with ZrO_2 only (10 wt%) and with Nb_2O_5 only (10 wt%), which were denoted as AuF, AuFZ and AuFN correspondingly. The Nb_2O_5 solution was prepared by dispersing Nb_2O_5 powder into 40 ml de-ionized water with the aid of ultrasound technique. Then an aqueous solution of $HAuCl_4$ (0.2 $mol \cdot l^{-1}$), $Fe(NO_3)_3 \cdot 9H_2O$ (1 $mol \cdot l^{-1}$) and $ZrOCl_2 \cdot 8H_2O$ (1 $mol \cdot l^{-1}$) was co-precipitated with an aqueous solution of K_2CO_3

1011-372X/06/0500–0131/0

($1\ mol \cdot l^{-1}$) and added to the Nb_2O_5 solution. The resulting brown suspension was aged at 60 °C under constant stirring for 1 h. After being centrifuged and washed several times until Cl^- was removed, the precipitates were dried at 120 °C for 8 h and calcined at 300 °C for 2 h in air.

2.2. Characterization methods

2.2.1. N_2 sorption

Surface areas were measured by the Brunauer-Emmett-Teller (BET) method using N_2 adsorption on a 'Quantachrome NOVA 4200e'instrument.

2.2.2. X-ray power diffraction

The XRD experiments were performed using Bruck D8 advance diffractometer. The XRD patterns were collected using Cu Kα radiation (0.1540 nm) at a voltage and current of 40 kV and 40 mA.

2.2.3. High resolution transmission electron microscopy (HRTEM)

High resolution transmission electron microscopy (HRTEM) analysis was performed using a JEOL 2010F (200 kV) microscope equipped with an EDS analytical system Oxford Link.

2.2.4. X-ray photoelectron spectroscopy (XPS)

The XPS measurements were performed with a Phi Quantum 2000 spectrophotometer with Al Kα radiation (1486.6 eV). The samples were preliminarily reduced at 150 °C for 9 h in hydrogen/nitrogen mixture (10 vol% H_2), and then were pressed into pellets and transferred to a test chamber. The spectra were collected with an analyzer using the pass energy of 29.35, 58.70, 117.40 and 29.35 eV for AuF, AuFZ, AuFN and AuFZN10, respectively. An electron takeoff angle of 45° was used. The vacuum in the test chamber was maintained below 1.33×10^{-7} Pa during the collection. Binding energies were corrected for surface charging by referencing them to the energy of C1s peak of contaminant carbon at 284.8 eV.

2.2.5. X-ray fluorescence analysis

The bulk composition was determined by X-ray fluorescence (XRF) analysis performed on 'PHILPS Magixpw2424 XRF' (Rh target, X-ray tube peak power 2.4 kW).

2.2.6. Temperature-programmed reduction (TPR)

H_2-TPR of the catalysts in fine powder form was carried out in a 'Micromeritics Autochem2910' instrument equipped with a thermal conductivity detector (TCD). Over 100 mg of the fresh sample was packed into a reactor with quartz tubing of 6 mm id., the reactor firstly purged with high purity helium gas at 120 °C for 1 h. TPR traces of sample was then pursued in a reductive flow of 30 ml/min 10 vol% H_2 in helium, heated at a rate of 5 °C/min from room temperature to 350 °C. The rate of hydrogen consumption was monitored by TCD of instrument.

2.3. Activity and stability measurement

Catalytic activity measurements were carried out by using 'CO-CMAT 9001 (HD. CO. LTD, Peiking, China)' at atmospheric pressure. A stainless steel tube with an inner diameter of 9 mm was used as the reactor tube. The samples were all 0.5 cm^3 (20–40 mesh size) in volume and preliminarily reduced at 1.50 °C for 9 h in hydrogen/nitrogen mixture (10 vol% H_2). The feed for the shift reaction was a 1:1 mixture of water vapor and model gas of reformed methanol (10 vol% CO, 60 vol% H_2, 12 vol% CO_2, 18 vol% N_2). Catalysts were tested in the range of 150–300 °C with a step size of 50 °C. At each test point the reaction temperature remained unchanged for 5 h. The flow rate was 91 $ml \cdot min^{-1}$ (space velocity: 11,000 h^{-1}). The concentration of CO in the effluent gas was on-line analyzed by a gas chromatograph (Shimadzu GC-8A). The catalytic activity of the samples at 200°C was recorded consecutively within 50 h at higher space velocity 22,000 h^{-1}. The activity was expressed by the degree of conversion of CO, which is defined as follows: $X(CO)\ (\%) = (1 - V'co/Vco) \times 100\%/(1 + V'co)$ where Vco and V′co are the inlet and outlet content of CO, respectively.

3. Results and discussion

3.1. Catalytic test

The catalytic performance of Au/Fe_2O_3 catalysts promoted with both ZrO_2 and Nb_2O_5, in comparison with AuF, AuFZ and AuFN samples is presented in Figure 1. It's clear that the addition of both ZrO_2 and Nb_2O_5 significantly enhanced the catalysts' activity over a wide temperature range. The enhancement was

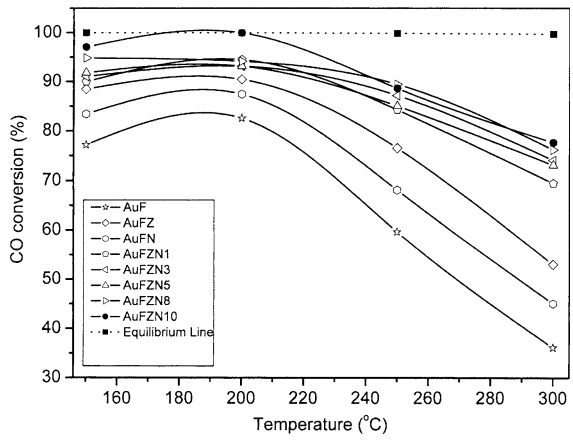

Figure 1. Temperature dependence of the WGS activity of the samples. Vapor–gas ratio: 1:1 (mol); space velocity: 11,000 h^{-1}.

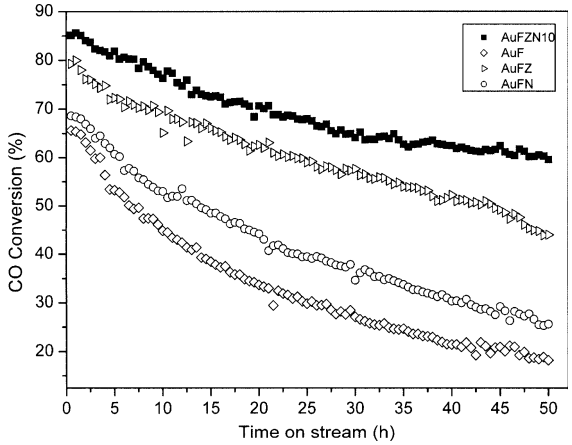

Figure 2. WGS activity at 200 °C as a function of time on stream: Vapor–gas ratio: 1:1 (mol); space velocity: 22,000 h^{-1}.

dramatic especially at higher temperatures. At 300 °C, all AuFZN samples exhibited a more than 100% increase in CO conversion compared to the unmodulated AuF formulation. Among the AuFZN samples with different Nb_2O_5 contents, AuFZN10 (10 wt% Nb_2O_5) was the most active. Its CO conversion almost reached the maximum value, namely the theoretical equilibrium value (99.9%) at 200 °C. The catalysts promoted with ZrO_2 or Nb_2O_5 only demonstrated some performance improvement as well, but to a less extent than the AuFZN series. Since there was the potential for undesirable side reactions to occur under WGS conditions, such as CO methanation, the outlet gas at 250 and 300 °C was expanded to a vacuum chamber and detected by IR instrument. However, methane, methanol or other byproducts were not detected for all the catalysts. Therefore the catalytic activities we obtained were creditable.

The time on stream results have provided further prove for the high activity and high stability of gold catalyst modified with zirconia and niobium oxide for WGS reaction in rich-hydrogen stream. Figure 2 shows the comparison of CO conversion on time on stream for AuF, AuFZ, AuFN and AuFZN10 samples at 200 °C with higher space velocity (22,000 h^{-1}). Though the CO conversion was drastically decreased within the first hours, AuFZN10 maintained its high activity very well ($60 \sim 70\%$ CO conversion) and kept stable after 30 h. The un-promoted AuF sample lost more than 50% of the original activity after 50 h on-stream, which is consistent with earlier studies [12]. The catalyst promoted with ZrO_2 or Nb_2O_5 only showed stable performance too, but their activity losses were greatly larger than that of AuFZN10. The effect of ZrO_2 is more noticeable compare to Nb_2O_5. Whereas when they co-exist, the effect is significant.

3.2. Catalysts characterizations

Change in the surface area and porous structure of unmodified and modified Au/Fe_2O_3 catalysts before and after the title reaction are presented in Table 1. It is obvious that the presence of ZrO_2 and Nb_2O_5 in the Au/Fe_2O_3 catalysts results in significant improvement of the BET surface area. All AuFZN samples showed a remarkable increase in surface area (around 200 $m^2 \cdot g^{-1}$),compared to the un-promoted AuF (120 $m^2 \cdot g^{-1}$). And to some extent, the addition of ZrO_2 or Nb_2O_5 increases the surface area of the fresh Au/Fe_2O_3 samples, they are 153 $m^2 \cdot g^{-1}$ and 136 $m^2 \cdot g^{-1}$, respectively. All the spent samples show a surface of about $30 \sim 70$ $m^2 \cdot g^{-1}$, indicating that serious sintering occurred during the catalytic operation. A similar tendency is followed by the pore volume values. The decreasing tendency for AuFZN samples, however, is slight less than those of other studied samples. The sintering of both Au particles and Fe_2O_3 particles could be more or less suppressed by the presence of ZrO_2 and Nb_2O_5 promoters.

XRD measurement was performed for reduced samples. As shown in Figure 3, two diffraction peaks related to the presence of magnetite and niobium oxide have been clearly observed. Because the small particle size usually leads to broad and weak diffraction peaks easily

Table 1.
Microstructural properties for samples

Samples	Fresh				Spent			
	S_{BET} ($m^2 \cdot g^{-1}$)	Average pore diameter (nm)	Total pore volume ($cm^3 \cdot g^{-1}$)	$d_{Fe_3O_4a}$	S_{BET} ($m^2 \cdot g^{-1}$)	Average pore diameter (nm)	Total pore volume ($cm^3 \cdot g^{-1}$)	$d_{Fe_3O_4b}$
AuF	120	3.13	0.34	11.2	33.8	14.91	0.26	19.4
AuFZ	152	2.82	0.19	10.1	53.7	9.22	0.17	14.8
AuFN	136	3.34	0.34	11.0	49.5	10.31	0.24	16.3
AuFZN1	200	3.13	0.23	10.9	65.7	6.05	0.25	14.5
AuFZN3	211	2.45	0.20	10.5	62.8	6.16	0.23	14.3
AuFZN5	199	1.87	0.18	9.8	67.3	5.82	0.19	13.9
AuFZN8	210	2.91	0.21	9.2	70.2	5.63	0.20	13.7
AuFZN10	218	3.06	0.24	8.9	73.5	5.54	0.22	12.9

$d_{Fe_3O_4a}$ andd_{Fe_3O4b}: the average diameter of magnetite crystallitesin.

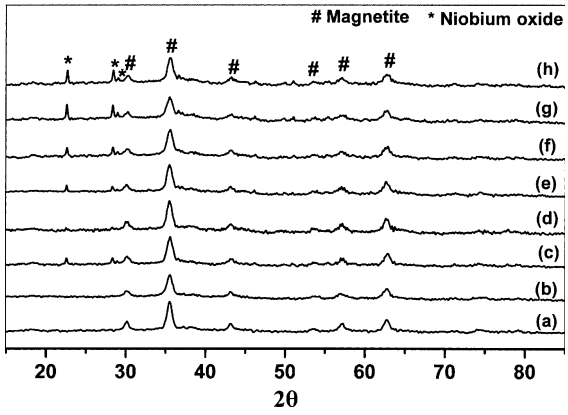

Figure 3. Power XRD patterns of Au/Fe_2O_3 catalysts after reduction (a) AuF, (b) AuFZ, (c) AuFN, (d) AuFZN1, (e) AuFZN3, (f) AuFZN5, (g) AuFZN8 and (h) AuFZN10.

lost in the background noise [7], the peaks of metallic Au was unable to be observed. The peak of ZrO_2 disappeared either, which indicated ZrO_2 exist in a state of high dispersion, or in an amorphous form. The interplanar spacing didn't change due to ZrO_2 and Nb_2O_5, which might suggest that they didn't enter the magnetite lattice. The average magnetite crystallite sizes as$d_{Fe_3O_4a}$ and$d_{Fe_3O_4b}$ (listed in table 1) estimated from the linewidth of Fe_3O_4 reflection peak ($2\theta \asymp 63$ °C) by using the Scherrer equation. For the ZrO_2 and Nb_2O_5 promoted catalysts, the degree of crystallinity of the magnetite decreased and the trend was stronger with increasing Nb_2O_5 loadings. The smaller values of$d_{Fe_3O_4a}$ the ZrO_2 and Nb_2O_5 containing catalysts lead us to the conclusion that these additives have a beneficial effect on the stabilization of small magnetite particles. According to the literature, the chemical composition of the supporting material or promoters can significantly influence the morphology of gold particles [14].

In order to further investigate this hypothesis, the AuFZN10 sample was studied in more detail by using electron microscopy (Figure 4). As shown in the TEM images, Au particles in the range of 2–6 nm are well isolated and highly dispersed on the supports, which is in good agreement with the assertion we made above. The existence of Nb_2O_5 particles on Fe_2O_3 support was verified by using EDS (energy dispersive spectroscopy) focusing on the regions containing highly contrast spots under transmission electron microscope.

The technique of XPS was employed to obtain information on the state of gold and iron in all reduced catalysts. Table 2 presents the XPS binding energy data for AuF, AuFZ, AuFN and AuFZN10 samples. Two distinct peaks due to the Au $4f_{7/2}$ and the Au $4f_{5/2}$ transitions are detected in Au 4f region for each sample. In particular, the Au $4f_{7/2}$ peaks is centred at 83.9 ± 0.1 eV, reflecting only a characteristic of metallic Au state for all the samples [15]. No oxidized form of gold was detected in all the samples, Zr 3d and Nb 3d spectra are similar to the standard ZrO_2 and Nb_2O_5 spectra, showing well resolved Zr^{4+} and Nb^{5+} lines, respectively. The combined use of the main Fe $2p_{3/2}$, Fe $2p_{1/2}$ lines and their satellites provide a reliable identification of Fe^{III} and Fe^{II} in Fe_3O_4 [16, 17], also in good agreement with the XRD results.

The near surface and bulk concentration of the elements determined by XPS and XRF measurements are listed in Table 3. Results indicate that the near surface concentration of gold atom is lower than the bulk concentration. AuFZN10 has the highest gold atomic near surface concentration (3.2 at %), while the gold concentrations are 2.1, 2.7 and 2.6 at % for AuF, AuFZ and AuFN samples, respectively. Since the catalytic activity of the supported Au catalysts is essentially regulated by the gold content exposed on the surface [18], the dramatic increase of the activity for AuFZN10 sample could be mainly ascribed to the higher number of gold active sites on the surface. The zirconia near surface concentration in AuFZNN10 is higher than the bulk of the catalyst. However, this work identifies new features of particular interest. The enrichment of Zr and

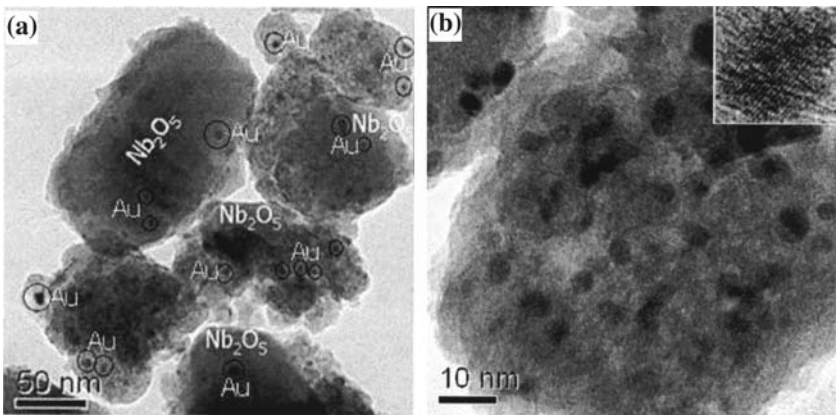

Figure 4. Low (a) and high (b) magnification TEM images of the AuFZN10 catalyst. The inset in figure 4b is a high resolution TEM image of a single Au nanoparticle.

Table 2.
Binding energies of Au4f, Fe2p, Zr3d and Nb3d

Sample	Binding energy (eV)							
	$Au4f_{7/2}$	$Au4f_{5/2}$	$Fe2p_{3/2}$	$Fe2p_{1/2}$	$Zr3d_{5/2}$	$Zr3d_{3/2}$	$Nb3d_{5/2}$	$Nb3d_{3/2}$
AuF	83.9	87.5	710.7	725.0	–	–	–	–
AuFZ	83.8	87.4	710.6	724.6	181.8	184.0	–	–
AuFN	83.8	87.5	710.6	724.1	–	–	206.8	209.6
ArFZN10	84.0	87.6	710.9	723.9	182.0	184.2	207.1	209.7

Table 3.
Surface and bulk atom concentration from XPS and XRF analysis

Samples	XPS (at %)				XRF (at %)			
	Au	Zr	Nb	Fe	Au	Zr	Nb	Fe
AuF	2.1	–	–	97.9	3.8	–	–	96.2
AuFZ	2.7	2.4	–	94.9	3.5	2.4	–	94.1
AuFN	2.6	–	0.6	96.8	3.8	–	5.1	91.1
AuFZN10	3.2	8.3	4.3	84.2	3.7	6.5	9.3	80.5

Nb also happened on the AuFZN10 surface. Compared to AuFZ (Zr: 2.4 at %) and AuFN (Nb: 0.6 at %), respectively, AuFZN10 sample has much higher Zr concentration (8.3 at %) and Nb concentration (4.3 at %). The cause of this phenomena maybe ascribed to the strong interaction between ZrO_2 and Nb_2O_5, which result from some strengthening in the metal–metal bonding [19]. On the other hand, the enhanced stability of AuFZN10 is mostly due to the presence of more surface Zr and Nb atoms, which help keep the particles apart and hence delay the sintering of catalysts. The change in the support particle size during the catalytic cycle was followed by XRD (summarized $asd_{Fe_3O_4}b$ in table 1). In general the magnetite particles sintered significantly during the reaction test. However, the magnetite crystallites of the catalysts that contain ZrO_2 and Nb_2O_5 seem more stable against sintering. This is responsible for the better stability shown by AuFZN samples.

The H_2-TPR results give another good proof for existing strong interaction between the ZrO_2 and Nb_2O_5. The H_2-TPR profiles of all the samples (Figure 5) investigated show a temperature peak below 85 °C, which is the reduction of Au_xO_y species and partial reduction of the iron cations present in the supported [20, 21]. The peak temperatures for AuF, AuFZ and AuFN are 83, 78 and 77 °C, respectively. As Nb_2O_5 content increases, this reduction peak shifts towards lower temperature and reaches the minimum value of 72 °C in AuFZN10 sample. Bond *et al.* proposed that for gold catalysts supported on metal oxides, a high dispersion of gold on the surface could promote the support reduction at lower temperature [22]. Therefore, the easier reduction of iron oxides in the AuFZN samples observed here could be accounted by a higher gold dispersion on the surface due to the addition of ZrO_2 and Nb_2O_5. Moreover, the other reduction peak in the range of 100–200 °C is also noteworthy. The peak for AuFN is similar to AuF, presenting at 177 °C. However, for the other samples, the peak shift to lower temperature and become broader with the presence of ZrO_2 and loading increasing Nb_2O_5. The similar reduction peaks for Au/Fe_2O_3 have also been reported by Fu *et al.* and Venugopal *et al.* They proposed that the hydrogen consumption seen in the temperature range (100–200 °C) is mainly due to the reduction of gold species [23, 24]. Interestingly, the performance of the catalysts has an intimate association with these

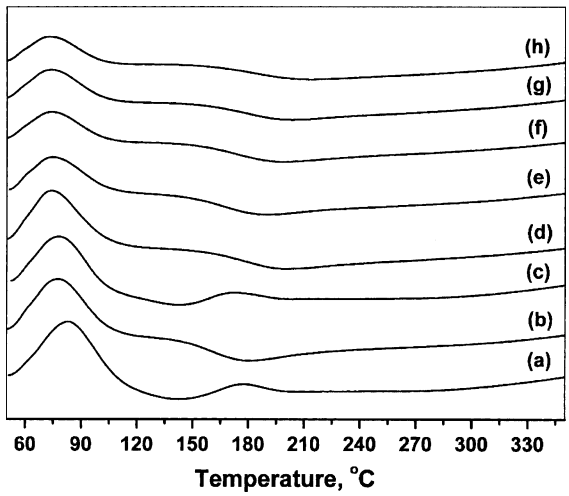

Figure 5. H_2-TPR profiles of Au/Fe_2O_3 catalysts (a) AuF, (b) AuFZ, (c) AuFN, (d) AuFZN1, (e) AuFZN3, (f) AuFZN5, (g) AuFZN8 and (h) AuFZN10.

reduction peaks. With the reduction peaks shifting to the lower temperature and becoming broader, the performance of the corresponding catalysts becomes higher. These phenomena indicate that the interaction of the Nb_2O_5 with the Au is weaker than that of ZrO_2 with the Au. In other words, the Nb_2O_5 alone can not efficiently enhance the performance of the Au/Fe_2O_3 catalysts. Only when ZrO_2 and Nb_2O_5 present together, the performance of the Au/Fe_2O_3 catalysts could be evidently improved.

According to the above XRD, TEM, XPS and TPR results, one can conclude that the catalytic behavior of the Au/Fe_2O_3 system is related to the gold species and structure and properties of the support. The activity in the low temperature region ($150 \sim 250$ °C) of the studied system is attributed to the gold species, the activity reaches its maximum at 200 °C; while the activity in the higher temperature region (> 250 °C) is attributed to the active magnetite phase [25]. If one increase the reaction temperature, the activity declines due to the growth of the gold species. On the other side, the increase of the degree of crystallinity of magnetite support implies the decrease of catalytic activity. As seen from figure 1, results show that the incorporation of ZrO_2 and Nb_2O_5 during co-precipitation may favor for gold dispersion and suppress the growth of magnetite crystallites during reaction step. It can be concluded that ZrO_2 and Nb_2O_5 act as structural promoters in Au/Fe_2O_3 catalyst.

4. Conclusion

In summary, we have developed an improved formulation of Au/Fe_2O_3 catalysts by adding the promoters ZrO_2 and Nb_2O_5. This is the first report of Au/Fe_2O_3 catalysts simultaneously modified by two promoters. The new catalyst exhibited significantly enhanced activity and stability for the low-temperature WGS reaction under the hydrogen-rich conditions. The results of characterizations obtained revealed ZrO_2 and Nb_2O_5 act as structural promoters. The doping process led to a progressive increase in the specific surface area and gold dispersion and decreased magnetite crystallite sizes. Moreover, the enrichment of Zr and Nb on the surface which induced by the strong interaction between ZrO_2 and Nb_2O_5 kept the particles apart delaying sintering which means better stability of AuFZN samples.

Acknowledgements

We would like to acknowledge the Department of Science of the People's Republic of China (Contact 20271012) for financial support.

References

[1.] W. Ruettinfer, O. Rlinich and R.J. Farrauto, J. Power Sources 118 (2003) 61.
[2.] E. Chenu, G. Jacobs, A.C. Crawford, R.A. Keogh, P.M. Patterson, D.E. Sparks and B.H. Davis, Appl. Catal. B 59 (2005) 45.
[3.] G. Jacobs, U.M. Graham, E. Chenu, P.M. Patterson, A. Dozier and B.H. Davis, J. Catal. 229 (2005) 499.
[4.] S.L. Swartz, M.M. Seabaugh, C.T. Holt and W.J. Dawson, Fuel Cell Bull. 4 (2001) 7.
[5.] D. Andreeva, V. Idakiev, T. Tabakova and A. Andreev, J. Catal. 158 (1996) 354.
[6.] D. Andreeva, T. Tabakova, V. Idakiev, P. Christov and R. Giovanoli, Appl. Catal. A 169 (1998) 9.
[7.] J.M. Hua, K.M. Wei, Q. Zheng and X.Y. Lin, Appl. Catal. A 259 (2004) 121.
[8.] F. Boccuzzi, A. Chiorino, M. Manzoli, D. Andreeva and T. Tabakova, J. Catal. 188 (1999) 176.
[9.] D. Andreeva, V. Idakiev, T. Tabakova, L. Ilieva, P. Falaras, A. Bourlinos and A. Travlos, Catal. Today 72 (2002) 51.
[10.] H. Sakurai, A. Ueda, T. Kobayashi and M. Haruta, Chem. Commun. (1997) 271.
[11.] T. Tabakova, F. Boccuzzi, M. Manzoli, J.W. Sobczak, V. Idakiev and D. Andreeva, Appl. Catal. B 49 (2004) 73.
[12.] C.H. Kim and L.T. Thompson, J. Catal. 230 (2005) 66.
[13.] A. Luengnaruemitchai, S. Osuwan and E. Gulari, Catal. Commun. 4 (2003) 215.
[14.] P. Konova, A. Naydenov, Cv. Venkov, D. Mehandjiev, D. Andreeva and T. Tabakova, J. Mol. Catal. A-Chem. 213 (2004) 235.
[15.] J.F. Moulder, W.F. Stickle, P.E. Sobol and K.D. Bomben, *Handbook of X-Ray Photoelectron Spectroscopy*, (Perkin-Elmer, Eden Prairie, 1992) p. 182.
[16.] C.R. Brundle, T.J. Chuang and K. Wandelt, Surf. Sci. 68 (1997) 459.
[17.] T. Tabakova, V. Idakiev, D. Andreeva and I. Mitov, Appl. Catal. A 202 (2000) 91.
[18.] F. Shi, Q.H. Zhang, Y.B. Ma, Y.D. He and Y.Q. Deng, J. Am. Chem. Soc. 127 (2005) 4182.
[19.] Y.S. Li, K.C. Wong, P.C. Wong and K.A.R. Mitchell, Appl. Surf. Sci. 103 (1996) 389.
[20.] A. Venugopal, J. Aluha and M.S. Scurrell, Catal. Lett. 90 (2003) 1.
[21.] J.M. Hua, Q. Zheng, Y.H. Zheng, K.M. Wei and X.Y. Lin, Catal. Lett. 102 (2005) 99.
[22.] G.C. Bond and D.T. Thompson, Catal. Rev. Sci. Eng. 41 (1999) 319.
[23.] Q. Fu, A. Weber and M. Flytzani-Stephanopoulos, Catal. Lett. 77 (2001) 87.
[24.] A. Venugopal and M.S. Scurrell, Appl. Catal. A 258 (2004) 241.
[25.] A. Andreev, V. Idaliev, D. Mihajlova and D. Shopov, Appl. Catal. 22 (1986) 385.